

Precise differential diagnosis of acute bone marrow edema and hemorrhage and trabecular microfractures using naïve and gamma correction pinhole bone scans

Journal of International Medical Research

2019, Vol. 47(4) 1493–1503

© The Author(s) 2019


Article reuse guidelines:

sagepub.com/journals-permissions

DOI: 10.1177/0300060518819910

journals.sagepub.com/home/imr



Yong-Whee Bahk¹, E. Edmund Kim^{2,3},
Yong-An Chung⁴ , Jung Mee Park¹,
Jeong Yong Jeon⁵ and Hyeonseok Jeong⁴

Abstract

Objective: To analyze the performance of sequential naïve pinhole bone scan (nPBS) and gamma correction pinhole bone scan (GCPBS), reinforced by ImageJ densitometry and pixelized microfracture measurement, for making specific diagnoses of bone marrow edema (BME), bone marrow hemorrhage (BMH), and trabecular microfractures (TMF).

Methods: We prospectively examined BME, BMH, TMF, and normal trabeculae in 10 patients using sequential nPBS and GCPBS. The intensity of ^{99m}technetium-hydroxydiphosphonate (^{99m}Tc-HDP) uptake was measured using a pixelized method and calculated using ImageJ densitometry in terms of arbitrary units (AU). This overall method was termed a visuospatial-mathematic assay (VSMA). We analyzed the ability of the calculated AU values to discriminate between the four states using GraphPad Prism software, with reference to previous morphological data.

Results: The calculated values were categorized as ≤ 50 AU for normal trabecula, 51–100 AU for BME, 101–150 AU for BMH, and ≥ 151 AU for TMF. The difference in uptake between normal

¹Department of Nuclear Medicine, College of Medicine, The Catholic University of Korea, Seoul, South Korea

²Department of Radiological Sciences, University of California, Irvine, USA

³Department of Nuclear Medicine, Seoul National University, Seoul, South Korea

⁴Department of Radiology, Incheon St. Mary's Hospital, College of Medicine, The Catholic University of Korea, Seoul, South Korea

⁵Department of Nuclear Medicine, Severance Hospital, Yonsei University College of Medicine, Seoul, South Korea

Corresponding author:

Yong-An Chung, 56 Dongsu-ro, Bupyeong-gu, Department of Radiology, Incheon St. Mary's Hospital, The Catholic University of Korea, Incheon, 21431, South Korea.
Email: yongan@catholic.ac.kr



trabecula and BME was significant and the differences among BME, BMH, and TMF were highly significant.

Conclusion: VSMA is a useful technique for refining objective individual diagnoses and for differentiating and quantitating BME, BMH, and TMF.

Keywords

Bone scintigraphy, bone marrow edema, bone marrow hemorrhage, trabecular microfracture, ImageJ densitometry, visuospatial-mathematic assay

Date received: 2 July 2018; accepted: 27 November 2018

Introduction

Bone marrow edema (BME), bone marrow hemorrhage (BMH), and trabecular microfractures (TMF) comprise a triad of fundamental pathological bone marrow changes that frequently occur as a result of trauma, sports injuries, osteoporosis, inflammation, infection, neoplasms, and even daily physical activities.¹ Precise imaging and systematic differential assays of each constituent of the triad is therefore considered essential for making a specific diagnosis in patients with bone marrow and trabecular diseases. TMF can be distinguished from BME and BMH by suppression of the blurry tracer uptake by BME and BMH using gamma correction pinhole bone scanning (GCPBS), and can be easily quantitated using a pixelized method (Figure 1).² Unfortunately, however, edema and hemorrhage cannot be distinguished from each other by this method because both are equally suppressed by gamma correction. To address this drawback, we aimed to calculate and compare the ^{99m}technetium-hydroxydiphosphonate (^{99m}Tc-HDP) uptake values of BME, BMH, and TMF using NIH ImageJ densitometry.

Recent studies revealed that the sequential use of naïve pinhole bone scans (nPBS) and GCPBS improved the differential

diagnosis of TMF in relation to BME and BMH in experiments in rats,² as well as in patients.³ Furthermore, NIH ImageJ densitometry has proven useful for the differential quantitation of ^{99m}Tc-HDP uptake among BME, BMH, and TMF,⁴ while pixelized measurement has been used to measure the precise size of TMF.⁵ We propose that the integrated use of sequential nPBS and GCPBS, together with NIH ImageJ densitometry and pixel measurement, collectively termed visuospatial-mathematic assay (VSMA), could help to differentiate among BME, BMF, and TMF.

In this study, we examined the use of VSMA for precisely differentiating among BME, BMF, and TMF, as validated by histological findings, and consider the usefulness and rationale of this technique in terms of providing high-quality images and rendering quantitative information for an accurate differential diagnosis.

Materials and methods

Clinical materials

We randomly sampled 95 1-cm² areas of normal trabeculae (n = 16), BME (n = 44), BMH (n = 23), and TMF (n = 12) examined by sequential nPBS and GCPBS in 10 consecutive patients. All participants

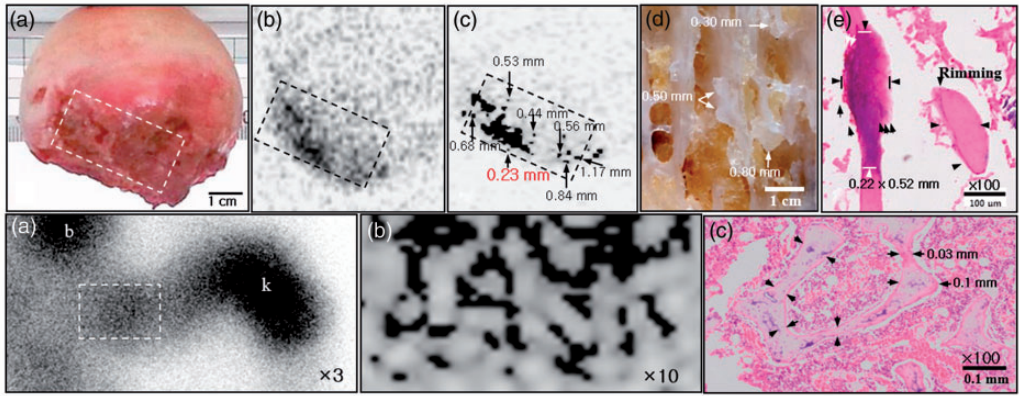


Figure 1. Histologically verified unsuppressed tracer uptake in osteoporotic trabecular microfractures in femoral head in a 92-year-old man. Femoral head was removed for bipolar prosthesis. Top panel: a Specimen shows roughened microfractures with seed-pearly calluses (frame). b Naïve pinhole scan shows blurry tracer uptake (frame). c Sequential gamma correction view shows suppressed blurry tracer uptake highlighting microfractures. Sizes measured using pixelized method. Smallest callus was 0.23 mm. d Surgical micrograph of sectioned specimen shows calluses. e Hematoxylin and eosin (H&E) stain shows a base stained 0.22 × 0.52 mm callus (arrowheads) with fine linear and meshy fractures (arrows) and endosteal rimming in a trabecula (paired arrows). Endosteal rimming in rats. Bottom panel: a Three-fold magnified pinhole scan shows trauma hypocenter (frame). k: knee, b: bladder. b Ten-fold magnified gamma correction pinhole bone scan shows unwashed diffuse tracer uptake in endosteal rimming in trabeculae due to hemorrhagic contusion. c H&E stain (×100) shows endosteal rimming (paired arrows) with hemorrhage and fat cells

underwent bone scintigraphy for trauma evaluation and were subsequently diagnosed with fractures, based on the results. This imaging study was approved by the Institutional Review Board of the College of Medicine, The Catholic University of Korea, which waived the need for patient consent. The patient who provided the surgical specimen in Figure 1 signed informed consent for its use.³

Sequential nPBS and GCPBS and reference conventional radiography

nPBS was carried out using a conventional pinhole scanning system (Signature e.cam; Siemens, Germany) equipped with a 4-mm pinhole collimator. The pinhole scan factors were 925 to 1110 MBq (25 to 30 mCi) ^{99m}Tc-HDP, 7-minutes scan time, and a 12-cm pinhole-aperture-to-object distance to encompass the bones of the major

joints, including the shoulder girdle, hip, knee, and distal tibiofibular syndesmosis. Gamma correction was performed by clicking the toolbars in the following sequence: ‘exposure’ and ‘auto-exposure’ to maximize uptake intensity, and ‘done’ and ‘save’ with a new name. The ‘exposure’ and ‘image-brightness’ were adjusted by increasing the gamma value from 50 (default) to 95, followed by ‘done’ and ‘save’ the finished image with another name. The use of the original naïve digital information and communications in medicine (DICOM) scan without image modification was strictly required. A reference conventional radiograph was taken in each case to provide fine topographic information on the studied bones using an x-ray machine (Axiom Aristo MX; Siemens) with exposure factors 65 to 70 kVp and 35 to 40 mAs with a 1-m source-image distance.

Densitometry analysis of ^{99m}Tc -HDP uptake intensity in BME, BMH, and TMF using sequential nPBS and GCPBS

NIH ImageJ densitometry (<http://rsb.info.nih.gov/ij>) was performed in each case to categorically quantify the levels of ^{99m}Tc -HDP uptake in BME, BMH, and TMF based on sequential nPBS and GCPBS. ^{99m}Tc -HDP uptake intensity was calculated using ImageJ densitometry in 95 randomly sampled 1-cm² areas of normal trabeculae (n = 16), BME (n = 44), BMH (n = 23), and TMF (n = 12). The results were expressed as arbitrary units (AU).

Measurement of TMF size based on unsuppressed ^{99m}Tc -HDP uptake

The size of the individual TMF based on unsuppressed ^{99m}Tc -HDP uptake was calculated using the pixelized method.⁵ Each micro-spot was appointed as a region of interest. The image profile was presented as a line spread function denoting the signal intensity of the applied line, with the y-axis indicating the signal intensity and the x-axis indicating the pixel number. To allow efficient measurement of the full width at half maximum, the matrix size was expanded to 512 × 512. Because of the increased number of pixels, the signal intensity value was assigned by interpolation at the expanded bin, which does not have a signal intensity value. Interpolation between the bins was achieved using the Gaussian curve fitting method with in-house MATLAB code (Mathworks, R2011a, Natick, MA, USA).^{5,6} The following equation was used for Gaussian curve fitting:

$$y(x) = \frac{1}{\sigma\sqrt{2\pi}} \exp\left[-\frac{(x-x_0)^2}{2\sigma^2}\right]$$

Where y = interpolated value, x = original frame value, x_0 = mean value of the frame value, and σ = standard deviation.

Differential ^{99m}Tc -HDP uptake intensities of BME and BMH using ImageJ densitometry

It is difficult to distinguish between BME and BMH by imaging, and gamma correction is unhelpful because it suppresses tracer uptake equally in both BME and BMH. However, ImageJ densitometry analysis of tracer uptake intensity⁴ allows precise quantification of the differential ^{99m}Tc -HDP uptake intensities in acute BME and BMH. We therefore examined the use of differential ImageJ uptake values (in terms of AU) for distinguishing between edema and hemorrhage based on 1-cm² regions of interest on sequential nPBS and GCPBS.

Histopathological validation

Histopathological validation was carried out using surgical specimens from patients with femoral neck fractures. Sectioned slices were stained with hematoxylin and eosin and examined under a microscope (×100; Canon, Tokyo, Japan). The histological findings and magnified GCPBS were compared for identification.

Statistical analysis

The uptake results for the 95 samples were analyzed statistically using GraphPad Prism software (San Diego, CA, USA). A value of $P < 0.05$ was considered significant (Student's t-test).

Results

^{99m}Tc -HDP uptake intensity was measured in 95 1-cm² areas of abnormal and normal trabeculae in 10 consecutive nPBS cases using NIH ImageJ densitometry. The 10 cases included six males and four females,

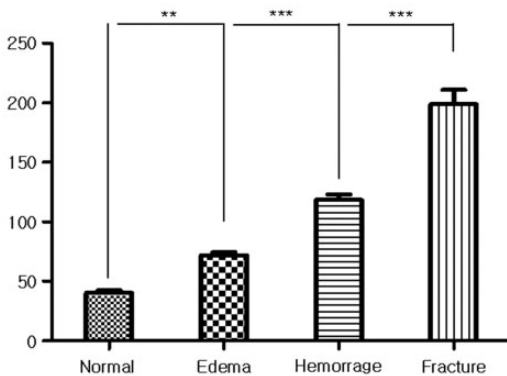
aged 16 to 71 years (mean 28.9 years). The lesions occurred in the bones of the shoulder girdle (n = 2), hip (n = 1), knee (n = 6), and distal tibiofibular syndesmosis (n = 1). The 95 assessed areas included BME (n = 44), BMH (n = 23), TMF (n = 12), and normal trabeculae (n = 16). Measurements were performed effectively in all but one TMF outlier, which had a value of 142.4 AU on nPBS, but this recovered to 155.6 AU after gamma correction. Hemorrhage in the bone marrow with concomitant TMF resulted in additional damage to already broken or contused trabeculae. BME with viscous blood along with phagocytic neutrophils and monocytes was presumed to be more injurious than low viscosity edema alone. The viscosity of edema is 1.27 ± 0.06 mPa.s and that of hemorrhagic blood is 3.26 ± 0.43 mPa.s.⁷ The lowest ^{99m}Tc-HDP uptake intensity was 10.8 AU in a normal trabecula and the highest uptake intensity was 243.2 AU in a microfracture. There was a significant difference in uptake values between normal trabeculae and BME ($P < 0.001$) and an even more significant difference among BME, BMH, and TMF ($P < 0.0001$) (Figure 2).

Differential diagnosis of BME and BMH using ImageJ densitometry

ImageJ densitometry was suitable for differentially assessing ^{99m}Tc-HDP uptake values in BME, BMH, and TMF. We attempt to differentiate between BME and BMH by unaided visual observation and using ImageJ densitometric assessment of uptake intensities in 1-cm² area on nPBS (Figure 3a). ^{99m}Tc-HDP uptake intensity was individually assessed in terms of AUs in each 1-cm² area. BME showed low tracer uptake on nPBS and BMH showed moderate tracer uptake, with mathematically calculated values of 73.8 AU and 120.2 AU, respectively. The calculated value for TMF was 207.8 AU, while GCPBS typically enhanced fracture uptake to 243.2 AU (Figure 3b).

No effect of BME on intact trabecula indicated by mild uptake on nPBS, suppressed by gamma correction

BME did not injure the trabecula and showed only mild tracer uptake, which was suppressed by gamma correction.



	AU	SD
Normal	40.38286	5.12296
Edema	71.98562	7.792942
Hemorrhage	118.5269	13.52758
Fracture	198.8583	33.94485

AU = arbitrary unit and SD = standard deviation.

** P value : < 0.001

*** P value : < 0.0001

Figure 2. Tracer uptake data for 95 samples analyzed using GraphPad Prism software. There was a significant difference in uptake values between normal trabeculae and edematous bone marrow (* $P < 0.001$) and an even more significant difference among edema, hemorrhage, and microfractures (** $P < 0.0001$). Table shows arbitrary units with standard deviation for normal, edematous, hemorrhagic, and fractured trabeculae

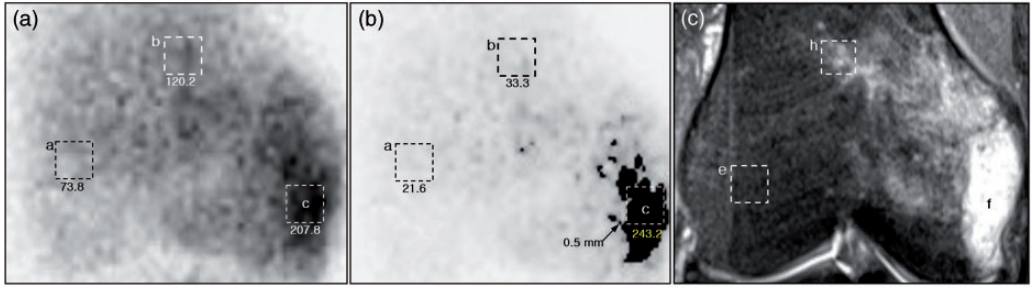


Figure 3. Edema and hemorrhage can be differentiated using gamma correction pinhole bone scan and ImageJ densitometry. a Naïve pinhole scan shows three 1-cm² areas of blurry tracer uptake in edema (a), hemorrhage (b), and fracture (c) with AU values of 73.8, 120.2, and 207.8 AU, respectively. b Gamma correction suppressed uptake in edema and hemorrhage, but highlighted uptake in fractures (c). Smallest fracture measured 0.5 mm.

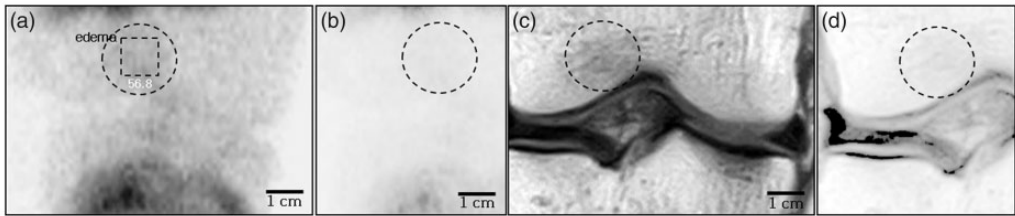


Figure 4. Edema has no injurious effect on trabeculae. Smallest edema in the current series occurred in the right femoral intercondylar fossa in a 16-year-old male student following a motor vehicle accident (circle). a Naïve ^{99m}Tc-HDP pinhole bone scan shows smallest 2-cm edema. Tracer uptake in unit area measured by ImageJ densitometry was 56.8 AU, close to the lowest value for edema. b Gamma correction view shows complete suppression of tracer uptake (circle). c Corroborative coronal T1-weighted (460/26) magnetic resonance (MR) image shows presence of edema with dark signal intensity (circle). d Gamma correction MR image shows suppression of dark signal MR intensity of edema (circle)

The smallest BME lesion in this series was 2 cm, occurring in the intercondylar fossa region of the right distal femur in a 16-year-old male student as the result of a motor vehicle accident (Figure 4a). ImageJ uptake intensity was 56.8 AU, which was in the lower range of edema, and this was suppressed by gamma correction (Figure 4b). Gamma correction was also applied to a corroborative T1-weighted MR image and showed suppression of edema as in GCPBS (Figures 4c, 4d). Further studies of gamma correction on MRI are currently underway.

Differential ImageJ densitometry intensity values for ^{99m}Tc-HDP uptake in BME, BMH, and TMF

The use of ImageJ densitometry AU values provided a useful quantitative scale of ^{99m}Tc-HDP uptake. The ^{99m}Tc-HDP uptake values calculated using ImageJ densitometry in sequential nPBS and GCPBS in 10 consecutive adult patients ranged from 10.8 AU in normal trabeculae to 243.2 AU in TMF. The uptake values were classified into four categories: ≤50 AU for normal trabeculae, 51 to 100 AU for BME, 101 to

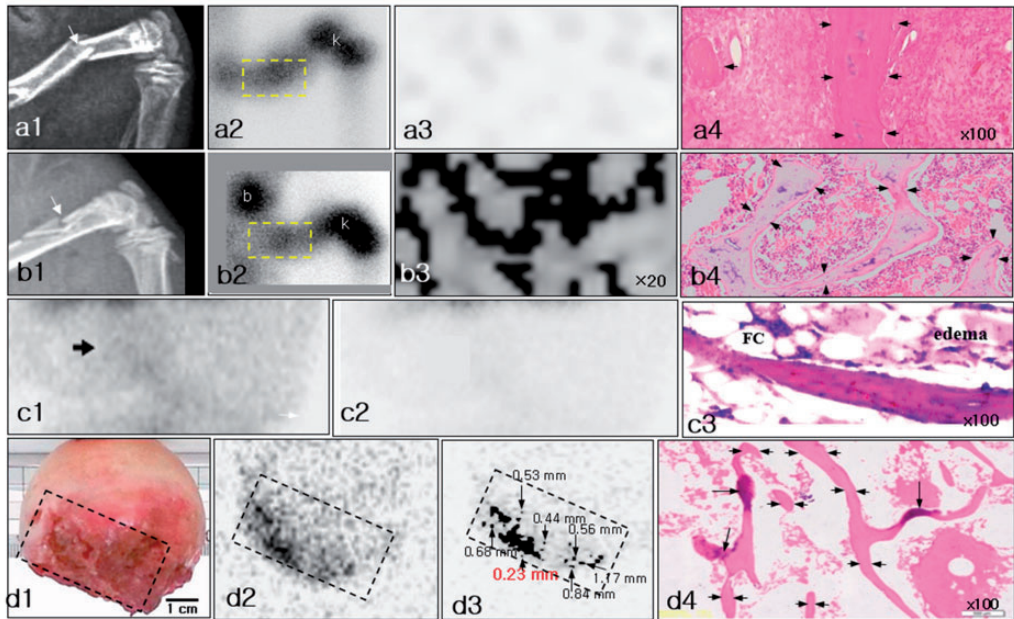


Figure 5. Gamma correction differentiates fracture from edema and hemorrhage. a1 #1 Rat radiograph shows femoral shaft fracture (arrow), based on a previous study.² a2 Naive pinhole scan shows hypocenter (frame). k: knee. a3 Gamma correction suppresses edema uptake. a4 Hematoxylin and eosin (H&E) staining shows intact trabecula with concomitant edema with hematopoietic and inflammatory cells but without rimming. b1 #2 Rat radiograph shows fracture (arrow). b2 Naive pinhole scan shows injured area (frame). b: bladder. b3 Gamma correction view shows enhanced uptake in endosteal rimming. b4 H&E stain shows hemorrhage and endosteal rimming. c1 Naive pinhole scan of right femoral condylar fossa shows faint edema uptake (arrow). c2 Gamma correction suppresses edema uptake. c3 H&E stain shows edema and fat cells with intact trabecula (teaching file case). FC: fat cell. d1 Specimen shows microfractures (frame). d2 Naive pinhole scan shows blurry uptake by bone marrow edema, bone marrow hemorrhage, and trabecular microfracture (TMF). d3 Gamma correction suppresses blurry uptake, highlighting microfractures. The smallest TMF measured 230 μm . d4 H&E stain shows endosteal rimming (paired arrows) and microfractures (single arrow) in bone marrow hemorrhage

150 AU for BMH, and ≥ 151 AU for TMF. There was one TMF outlier according to AU value, with an uptake intensity of 142.4 AU on nPBS, but this recovered to 155.6 AU after gamma correction.

No effect of BME on intact trabecula and injurious effect of BMH on broken trabecula

BME had no injurious effect on intact trabecula (Figure 5 top and third panels), but BMH was associated with or accompanied by TMF or endosteal rimming, with

unsuppressed high $^{99\text{m}}\text{Tc}$ -HDP uptake in both rats in previous histological experiments² and in patients in the current study³ (Figure 5 second and bottom panels). These results suggested that BME did not injure the trabecula, whereas BMH caused additional damage to already injured trabeculae.

Histological validation of additive damage by BMH to already fractured trabeculae

Additional injury to already fractured trabeculae through the phagocytic action of neutrophils, monocytes, and other blood

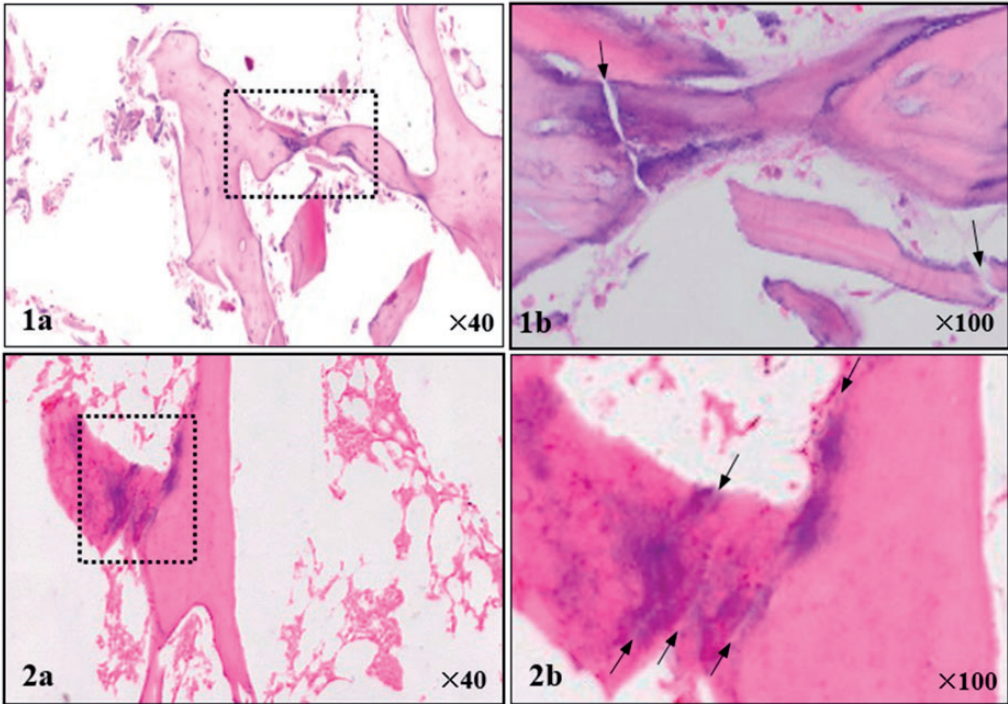


Figure 6. Hematoxylin and eosin stain shows trabecular microfractures in surgical specimens of femoral neck fractures in two patients. Top panel. 1a low-power view ($\times 40$); 1b high-power view ($\times 100$). Bottom panel. 2a low-power view; 2b high-power view. Low-power views show base stain and high-power views show microfractures

components was considered to cause BMH with concomitant TMF. TMF heals by osteoneogenesis, involving callus formation and/or endosteal rimming, into which $^{99m}\text{Tc-HDP}$ was actively incorporated (Figure 5b, d)^{2,3}. Endosteal rimming showed high unsuppressed tracer uptake in thickened endosteum, and TMF was imaged as pinpointed, speckled, round, ovoid, rod-like, linear, and geographic areas of high $^{99m}\text{Tc-HDP}$ uptake, which were not suppressed by gamma correction. Endosteal rimming and TMF were verified by hematoxylin and eosin staining. The region of interest was initially characterized by base staining under low-power microscopy (Figure 6 top panel), and microfractures within the callus were

confirmed by high-power microscopy (Figure 6 bottom panel).

Discussion

Recent developments in GCPBS have made it necessary to devise a quantitative method for assessing $^{99m}\text{Tc-HDP}$ uptake to allow the precise morphobiochemical evaluation of BME, BMH, and TMF.^{2,3,8} We therefore designed the VSMA to specifically visualize, distinguish, and quantitate BME, BMH, and TMF using sequential nPBS and GCPBS, NIH ImageJ densitometry, and pixelized measurement. TMF, BME, and BMF are fundamental histopathological changes that occur ubiquitously in cases of trauma, sports injury, osteoporosis,

inflammation, infection, neoplasms, and other bone diseases, as well as during daily physiological activities. TMF involves minute fractures of the bone trabeculae, while BME is the accumulation of increased clear serous fluid in the bone marrow, and BMH involves the accumulation of extravasated blood. BME alone does not cause trabecular injury, but BMH may cause additional damage to already injured trabeculae. The current study focused on acute BME and BMH, as well as acute TMF. ImageJ densitometry calculated that normal trabecula had an uptake of ≤ 50 AU, compared with 51 to 100 AU for edema, 101 to 150 AU for hemorrhage, and ≥ 151 AU for TMF. According to GCPBS, the smallest TMF was 0.23 mm.

We previously showed that acute bone contusion induced endosteal rimming with unsuppressed high ^{99m}Tc -HDP uptake in rat trabeculae,² while a similar study in surgical specimens from patients with femoral neck fractures showed that fractures were also associated with unsuppressed high ^{99m}Tc -HDP uptake in seed-pearly microcalluses, which were acutely formed in TMF.³ Yamamura⁹ showed that hemorrhage transformed fatty marrow into a bone-forming tissue in a dog model, while Majkowski et al.¹⁰ confirmed that hemorrhage induced changes in the shear strength of the cement-bone interface in cattle, and an arthroscopic study by Rangger et al.¹¹ showed a link between trabecular fractures and hemorrhage in fatty bone marrow. These previous studies demonstrated that simulated and actual hemorrhage could injure trabeculae, resulting in osteoneogenesis via endosteal rimming and/or seed-pearly callus formation. Callus formation in TMF is considered to be associated with additional injurious effects in already injured trabeculae, which are vulnerable to intrinsic hemorrhage. The increased ^{99m}Tc -HDP uptake in acute TMF has been demonstrated radiobiochemically and

scintigraphically to be due to the avid biochemical incorporation of bone tracer into amorphous calcium phosphate in the injured bone, while the suppressed uptake in BME and BMH is ascribed to ^{99m}Tc -HDP adhesion to crystalline hydroxyapatite.^{2,8,12}

MR imaging is widely used in the clinic for studying BME,^{13–18} but its use for BMH is limited.^{19,20} This discrepancy is considered to be due to the technical difficulty of specific MR imaging of BMH and its interpretation. In this connection, the histopathology–MRI correlation study by Zanetti et al.¹⁸ reported only “edema-like” change, with no reference to hemorrhage despite the presence of small bleeding areas in a case of chronic arthritis-related bone marrow disease. BME, BMH, and TMF can now be distinguished using VSMA. Indeed, this method allowed four different uptake patterns corresponding to normal trabeculae, BME, BMH, and TMF to be distinguished and categorized, with the lowest uptake (0.8 AU) in normal trabeculae and the highest (243.2 AU) in TMF. VSMA was thus useful for morphologically and quantitatively distinguishing among BME, BMH, and TMF. In particular, BME could be distinguished from BMH both visually and in terms of tracer uptake, with mild ^{99m}Tc -HDP uptake in edema and moderate uptake in hemorrhage, with an objective difference according to ImageJ densitometry calculations.

The AU classification of ImageJ densitometry was based on three factors: TMF was highlighted as such by GCPBS imaging; ImageJ densitometry permitted easy and precise measurements of ^{99m}Tc -HDP uptake in sequential nPBS and GCPBS; and the injurious effect of more viscous hemorrhaged blood was considered to be greater than that of less viscous edema. The viscosity of edema has been shown to be 1.27 ± 0.06 mPa.s compared with 3.26 ± 0.43 mPa.s for blood, with the latter

containing phagocytic neutrophils and monocytes.

Pivonka and Dunstan²¹ published a mathematical model of bone-fracture healing. Their four-phase model consisted of an inflammatory phase, two repair phases with soft callus formation followed by hard callus formation, and a physiological remodeling phase. Their results indicated that environmental conditions, such as blood supply and the availability of mesenchymal stem cells, were crucial for fracture healing. In this connection, we suggest that precise imaging of BME, BMH, and TMF and the regular quantitation of bone metabolic change, for example in terms of AU, could significantly improve the diagnosis and treatment of MBE, BMH, and TMF.

There were some limitations to this study. First, the statistical power was limited due to the relatively small sample sizes. Second, ImageJ densitometry is currently not widely used in medical imaging analysis. Our findings need to be confirmed in future studies with larger sample sizes, and using a more widely available method such as lesion-to-background uptake ratio.

In summary, BME, BMH, and TMF can be finely imaged and differentially diagnosed using VSMA, which consists of sequential nPBS and GCPBS assessment, tracer uptake assessment using NIH ImageJ densitometry, and pixelized measurement. VSMA can distinguish BME from BMH, and can distinctly demonstrate TMF. Radiobiochemically, ^{99m}Tc-HDP uptake in normal trabeculae, BME, and BMH was suppressed by gamma correction, while tracer uptake in TMF was contrarily enhanced. Normal trabeculae, BME, BMH, and TMF could be distinctly classified by discrete ranges of uptake values. In conclusion, BME, BMH, and TMF may be differentially diagnosed by VSMA in the absence of MRI, with the provision of useful information for evaluating traumatic bone marrow injuries.

Declaration of conflicting interest

The authors declared no potential conflicts of interest with respect to the research, authorship, and/or publication of this article.

Funding

The authors disclosed receipt of the following financial support for the research, authorship, and/or publication of this article: This study was supported by the National Research Foundation of Korea (NRF) funded by the Ministry of Science and ICT (2015M3C7A1064832).

ORCID iD

Yong-An Chung  <http://orcid.org/0000-0003-4004-4019>

References

1. Salcianu IA, Bratu AM, Bondari S, et al. Bone marrow edema - premonitory sign in malignant hemopathies or nonspecific change? *Rom J Morphol Embryol* 2014; 55: 1079–1084. 2015/01/22.
2. Bahk Y-W, Chung Y-A, Lee U-Y, et al. Gamma correction ^{99m}Tc-hydroxymethylene diphosphonate pinhole bone scan diagnosis and histopathological verification of trabecular contusion in young rats. *Nucl Med Commun* 2016; 37: 988–991.
3. Bahk YW, Hwang SH, Lee UY, et al. Morphobiochemical diagnosis of acute trabecular microfractures using gamma correction ^{99m}Tc-HDP pinhole bone scan with histopathological verification. *Medicine (Baltimore)* 2017; 96: e8419. 2017/11/16. DOI: 10.1097/MD.00000000000008419.
4. National Institute of Health. ImageJ, <http://rsb.info.nih.gov/ij>.
5. Jung JY, Cheon GJ, Lee YS, et al. Pixelized measurement of (^{99m}Tc)-HDP micro particles formed in gamma correction phantom pinhole scan: a reference study. *Nucl Med Mol Imaging* 2016; 50: 207–212. 2016/08/20. DOI: 10.1007/s13139-015-0391-8.
6. Yoon D-K, Jung J-Y, Jo Hong K, et al. Tomographic image of prompt gamma ray from boron neutron capture therapy: a

- Monte Carlo simulation study. *Appl Phys Lett* 2014; 104: 083521.
7. Rosenson RS, McCormick A and Uretz EF. Distribution of blood viscosity values and biochemical correlates in healthy adults. *Clin Chem* 1996; 42: 1189–1195. 1996/08/01.
 8. Bahk YWCY. Gamma correction 99mTc-HDP scan diagnosis of trabecular microfracture and contusion. In: YW B (ed.) *Combined Scintigraphic and Radiographic Diagnosis of Bone and Joint Diseases Including Gamma Correction Interpretation*. 5th ed. Berlin: Springer-Verlag, 2017, pp.649–688.
 9. Yamamura M. [Structural changes in jaw bone marrow after hemorrhagic infiltration]. *Kokubyo Gakkai Zasshi* 1994; 61: 207–220. 1994/06/01.
 10. Majkowski RS, Bannister GC and Miles AW. The effect of bleeding on the cement-bone interface. An experimental study. *Clin Orthop Relat Res* 1994; 299: 293–297. 1994/02/01.
 11. Rangger C, Kathrein A, Freund MC, et al. Bone bruise of the knee: histology and cryosections in 5 cases. *Acta Orthop Scand* 1998; 69: 291–294. 1998/08/14.
 12. Francis MD, Ferguson DL, Tofe AJ, et al. Comparative evaluation of three diphosphonates: in vitro adsorption (C-14 labeled) and in vivo osteogenic uptake (Tc-99m complexed). *J Nucl Med* 1980; 21: 1185–1189.
 13. Eustace S, Keogh C, Blake M, et al. MR imaging of bone oedema: mechanisms and interpretation. *Clin Radiol* 2001; 56: 4–12. 2001/02/13. DOI: 10.1053/crad.2000.0585.
 14. Korompilias AV, Karantanas AH, Lykissas MG, et al. Bone marrow edema syndrome. *Skeletal Radiol* 2009; 38: 425–436. 2008/07/17. DOI: 10.1007/s00256-008-0529-1.
 15. Kubo T, Yamamoto T, Inoue S, et al. Histological findings of bone marrow edema pattern on MRI in osteonecrosis of the femoral head. *J Orthop Sci* 2000; 5: 520–523. 2001/02/17.
 16. Starr AM, Wessely MA, Albastaki U, et al. Bone marrow edema: pathophysiology, differential diagnosis, and imaging. *Acta Radiol* 2008; 49: 771–786. 2008/07/09. DOI: 10.1080/02841850802161023.
 17. Thiryayi WA, Thiryayi SA and Freemont AJ. Histopathological perspective on bone marrow oedema, reactive bone change and haemorrhage. *Eur J Radiol* 2008; 67: 62–67. 2008/03/14. DOI: 10.1016/j.ejrad.2008.01.056.
 18. Zanetti M, Bruder E, Romero J, et al. Bone marrow edema pattern in osteoarthritic knees: correlation between MR imaging and histologic findings. *Radiology* 2000; 215: 835–840. 2000/06/01. DOI: 10.1148/radiology.215.3.r00jn05835.
 19. Mink JH and Deutsch AL. Occult cartilage and bone injuries of the knee: detection, classification, and assessment with MR imaging. *Radiology* 1989; 170: 823–829. 1989/03/01. DOI: 10.1148/radiology.170.3.2916038.
 20. Ryu KN, Jin W, Ko YT, et al. Bone bruises: MR characteristics and histological correlation in the young pig. *Clin Imaging* 2000; 24: 371–380. 2001/05/23.
 21. Pivonka P and Dunstan CR. Role of mathematical modeling in bone fracture healing. *Bonekey Rep* 2012; 1: 221. 2012/01/01. DOI: 10.1038/bonekey.2012.221.